Advances in Environmental Technology 2 (2018) 83-93

Advances in Environmental Technology

journal homepage: http://aet.irost.ir

Keratin nanoparticles: synthesis and application for Cu(II) removal

Seyedeh Zahra Mousavi[a], Mehrdad Manteghian[a,*], Seyed Abbas Shojaosadati[b], Hassan Pahlavanzadeh[a]

[a] *Department of Chemical Engineering, Tarbiat Modares University,Tehran, Iran*

[b] *Biotechnology Group, Department of Chemical Engineering, Tarbiat Modares University, Tehran, Iran*

ARTICLE INFO

Article history:
Received 13 June 2018
Received in revised form
19 September 2018
Accepted 25 September 2018

Keywords:
Chicken feather
Keratin nanoparticle
Biosorbent
Adsorption isotherm
Cu(II) removal

ABSTRACT

A straightforward procedure to synthesize keratin nanoparticles (KNP) from chicken feathers was introduced. The characterization of the synthesized nanoparticles was done using Fourier transform infrared (FTIR) spectroscopy, dynamic light scattering (DLS), X-ray diffraction (XRD) patterns and transmission electron microscopy (TEM). The FTIR analysis revealed no significant chemical change after the nanoparticle synthesis. TEM imaging indicated the synthesis of KNPs with a spherical morphology and mean size of 42 nm. The DLS results indicated that the synthesized KNPs were stable in aqueous media by having a zetapotential of lower than -30 mV. The produced KNPs were then evaluated for the biosorption of Cu (II) from aqueous solutions. The analyzed adsorption isotherm data revealed the change from a Redlich-Peterson isotherm to a Langmuir one by increasing the biosorbent dosage, which could be attributed to the more prepared adsorption sites. The experiments of the effect of the biosorbent dosage suggested the best removal at a KNP dose of 3.0 g/L. At this dosage, the maximum Cu (II) adsorption capacity and Langmuir constant were 50 mg/g and 10.8×10^{-3} L/mg, respectively; the adsorption kinetic followed the pseudo-second order model.

1. Introduction

Heavy metal pollution in the water ecosystem is one of the most important environmental issues [1]. Among different heavy metals, copper is widely used in various industries such as electrical, dying, fertilizer, electroplating and petroleum [2,3]. Copper is not biodegradable and accumulates in living organisms. It can disturb biological functions if it exceeds the established tolerance limit [4-6]. The World Health Organization (WHO) reported the maximum limit of copper in drinking water to be 2 mg/L in order to prevent potential health problems [7]. Different approaches have been developed for heavy metal removal including chemical precipitation, ion exchange, nanofiltration, reverse osmosis and adsorption [8-10]. The adsorption process is more popular than the other separation methods due to its simplicity, relative low cost and high efficiency. Biopolymers are emerging adsorbents for heavy metal removal [11-13]. Keratin which is abundant in chicken feathers (91% keratin, 8% water and 1% lipids) is a natural biopolymer that can be used for this purpose. Keratin is a fibrous protein and has approximately 7-20% cysteine residue [14]. The high amount of cysteine with thiol groups creates inter- and intra-molecular disulfide bonds. These bonds give keratin a strong structure and make it unsolvable in polar and non-polar solvents as well as weak acids and bases. Keratin also has a great quantity of hydroxyl amino acids, especially serine, and a large number of amino acids containing $-NH_2$ and $-COOH$ functional groups. Originating from such amino acids, keratin is applicable as a biosorbent for the removal of heavy metal and dye from aqueous solutions [15-19]. Recently, nanoparticles have attracted the interest of many researchers due to their high surface area, low diffusion resistance and more active sites [20]. Considering the advantages of nanoparticles and keratin biosorbents, keratin nanoparticles were synthesized in this study. They were then used for copper removal and the adsorption

*Corresponding author. Tel: +98-21-82883333
E-mail address: manteghi@modares.ac.ir
DOI: 10.22104/AET.2018.2948.1143

isotherm and kinetics were studied to understand the mechanism of the biosorption process.

2. Materials and methods

2.1. Materials

The following materials were used in this study : steam-treated sterilized chicken feathers (SCF, provided by local processing plants); sodium hydroxide (≥99.0%) hydrochloric acid 37%, acetic acid glacial and nitrate salt of copper ($Cu(NO_3)_2.3H_2O$) that were purchased from the Merck Co.; and Tris(hydroxymethyl)aminomethan which was purchased from the SinaClon Co. All the chemicals were of analytical grade and used without further purification.

2.2. Methods

2.2.1. Keratin extraction

Keratin extraction was done according to the Nomura method [21]. Briefly, 10 g of the chopped SCF was hydrolyzed with 300 ml of 0.3 N NaOH solution. The mixture was blended for 48 h at room temperature (25°C). The extracted solution was centrifuged at 4000 rcf for 15 min which was followed by filtration to separate undissolved materials. The filtrate was precipitated by adjusting the pH to 4.2, the isoelectric point of keratin, using 1N hydrochloric acid. It was then centrifuged at 4000 rcf for 20 min. The precipitated keratin was washed several times to become neutral. The extracted keratin powder (EKP) was dried at -48 °C for 12 h.

2.2.2. KNP synthesis

The solubility of keratin in water was significantly improved by adding a Tris base which created a relatively mild alkaline condition. The ratio of the Tris base to the keratin weight was chosen to be 0.09 (according to the experiments which were performed to find the optimum ratio). The mixture of keratin and Tris base in water were stirred at 400 rpm for 16 h under room temperature. This made the particles smaller. It was then sonicated (300 W, 10 min) with a probe ultrasonic device (UP400-A, the Ultrasonic Technology Development Company) to break the microparticles into nanoparticles. The generated KNPs could be stored under 4°C before use. They could also be freeze dried at -48 °C for 6 h, and be used in a solid form.

2.2.3. Characterization

The FTIR spectroscopy of SCF, freeze dried EKP and produced KNPs were recorded with the spectrophotometer (Spectrum 100, Perkin Elmer) at the frequency range of 4000-400 cm^{-1}. XRD was also conducted (x-ray generator, Philips) to determine the chemical changes after the keratin extraction. The size measurement of KNP was done by a particle size analyzer (Zetasizer, Malvern). The morphology of the magnetic particles was characterized with TEM (LEO 906, 80 kV). Negative staining was applied for TEM imaging. The KNPs were sonicated for 3 min, then a drop of the sample was placed on a carbon copper grid, dried at room temperature and observed under TEM.

2.2.4. Batch adsorption experiments

The stock solution of Cu (II) (1000 mg/L) was prepared by copper nitrate salt. Different doses of KNP (0.1-5.0 g/L) were added to the Cu (II) solution of 100 mg/L to find the optimum biosorbent dosage. The samples were shaken for 1 h to reach equilibrium. After adding the KNPs to the Cu (II) solution, adsorption by negative charged KNPs occurred. This caused the KNPs to become neutral and KNP precipitation was observed after sorption. The precipitated KNPs could be simply separated by filtration or centrifugation. The obtained optimum KNP dose, which was based on the maximum Cu (II) removal, was used for further adsorption experiments. SCF was also tested at the optimum biosorbent concentration for comparison. The residual Cu (II) concentration was measured by a flame *atomic absorption spectrophotometer* (*Shimadzu AA-670*). Since Cu (II) precipitation occurs at a pH of more than 5, the sorption experiments were performed at a pH of 5. So, metal precipitation does not interfere with biosorbent function [22-24].

2.2.5. Adsorption isotherm

The Cu (II) stock solution was diluted in the range of 40-400 mg/L to study the adsorption isotherm at an ambient temperature of 25 °C and a pH value of 5. Three different adsorbent doses of 0.15, 1.5 and 3.0 g/L were studied for the adsorption isotherm experiments. The following equation could be applied to calculate the adsorption capacity of Cu (II) at equilibrium [25]:

$$q_e = \frac{V(C_0 - C_e)}{m} \quad (1)$$

The removal of Cu (II) was calculated according to the following equation [25]:

$$R(\%) = \frac{C_0 - C_e}{C_i} \times 100 \quad (2)$$

where C_0 and C_e (mg/L) were the initial and equilibrium concentrations of Cu(II), V (L) was the volume of the solution, and m (g) was the mass of biosorbent. The interaction between Cu (II) and biosorbent was expressed by adsorption isotherm models. For this purpose, the two parameter adsorption isotherm models of Langmuir and Freundlich, as well as the three parameter models of Sips and Redlich-Peterson, were studied.

2.2.5.1. Langmuir isotherm

The Langmuir model is represented by the following equation [26]:

$$q_e = \frac{K_L q_m C_e}{1 + q_m C_e} \quad (3)$$

where q_e denotes the amount of metal adsorbed per unit mass of biosorbent (mg/g), C_e refers to the copper concentration at equilibrium (mg/L), K_L is Langmuir constant (L/g), and q_m is the maximum adsorption capacity of the biosorbent (mg/g). The separation factor (R_L) is a dimensionless constant which can be expressed as:

$$R_L = \frac{1}{1 + K_L C_0} \quad (4)$$

where C_0 is the initial metal concentration (mg/L). The value of R_L indicates whether the adsorption is unfavorable (R_L>1), linear (R_L=1), favorable (0<R_L<1) or irreversible (R_L=0).

2.2.5.2. Freundlich isotherm

The Freundlich isotherm model, which is an empirical model, can be expressed by the following relationship [27]:

$$q_e = K_F {C_e}^{1/n} \quad (5)$$

where K_F (mg/g) and n are the Freundlich constants related to the adsorption capacity and intensity, respectively.

2.2.5.3. Redlich-Peterson isotherm

The Redlich-Peterson isotherm is a three parameter model combining the features of the Langmuir and Freundlich isotherms. It can be represented as [28]:

$$q_e = \frac{K_{RP} C_e}{1 + a_{RP} {C_e}^{\beta_{RP}}} \quad (6)$$

where K_{RP} (L/mg), a_{RP} and β_{RP} are Redlich-Peterson constants. When the value of $a_{RP}{C_e}^{\beta_{RP}}$ is much bigger than 1 (β_{RP} tends to zero) this isotherm reduces to the Freundlich model. It also reduces to the Langmuir isotherm in the cases where β_{RP} approaches to 1. The ratio of K_{RP}/a_{RP} represents the adsorption monolayer capacity.

2.2.5.4. Sips isotherm

The Sips equation includes three parameters and is a combination of the Langmuir and Freundlich isotherms. It can be expressed as [29]:

$$q_e = \frac{K_S {C_e}^{\beta_S}}{1 + a_S {C_e}^{\beta_S}} \quad (7)$$

where K_S (L/mg), a_S and β_S are Sips constants. The equation reduces to the Langmuir isotherm when β_S equals to 1 and it reduces to the Freundlich isotherm at low concentrations of the adsorbate.

2.2.6. Adsorption kinetics

The adsorption kinetics was studied at the Cu (II) initial concentration of 100 mg/L and pH value of 5. The pseudo-first [30] and pseudo-second order [31] rate equations, as well as the intra-particle diffusion model [32], were applied to model the kinetics of Cu (II) adsorption on KNP. These models are represented in Equations (8-10):

$$\ln(q_e - q_t) = \ln q_e - k_1 t \quad (8)$$

$$\frac{t}{q_t} = \frac{1}{k_2 q_e^2} + \frac{1}{q_e} t \quad (9)$$

$$q_t = k_3 t^{1/2} + k_d \quad (10)$$

where q_e and q_t (mg/g) are the adsorption capacities at equilibrium and time t; k_1 (min^{-1}), k_2 (g mg^{-1} min^{-1}) and k_3 (mg g^{-1} $min^{-1/2}$) are pseudo-first order, pseudo-second order and intra-particle diffusion rate constants; and k_d (mg/g) is the intra-particle diffusion model intercept.

3. Results and discussion

3.1. Characterization

3.1.1. FTIR spectroscopy

The FTIR spectra of SCF, EKP and KNP are shown in Figure 1 to investigate the secondary structure of the protein. The bands in the wave numbers of 3298, 3399 and 3349 cm^{-1} of SCF, EKP and KNP, respectively, and in the wave numbers of about 2990 cm^{-1} are due to N–H hydrogen bond stretching related to amide A and amide B [33]. Although both bands represent N–H hydrogen bond stretching, amide B is weaker than amide A. The bands at 1638, 1659 and 1647 cm^{-1} (of SCF, EKP and KNP) are correlated with the C═O stretching of amide I. The shift of amide I to higher wave numbers infers the increase of disordering structures [34]. The wave numbers at 1528, 1532 and 1547 cm^{-1} (of SCF, EKP and KNP) correspond to the secondary N–H bending of amide II. The bands at 1230, 1235 and 1285 cm^{-1} (of SCF, EKP and KNP) are as a result of C–N stretching in amide III [35,36]. The bands of amide I and amide II suggest the presence of α-helices in KNP structure; while amide III represents β-sheet structures with weak intensity. In the EKP sample, a small shift at wave numbers of 3300 cm^{-1} toward higher wave numbers is seen. This shift corresponds to some hydrogen bond disruption after the keratin extraction process [17]. As no shift is seen in the KNP sample, disrupted bonds are likely regenerated. The bands in the range of 2581 to 2962 cm^{-1} are related to CH_2 and CH_3 stretching vibration. The bands at 640, 667 and 630 cm^{-1} are assigned to the C-S bond stretching vibration [33].

3.1.2. XRD

The wide-angle XRD patterns of SCF, EKP and KNP are shown in Figure 2. There are two distinct peaks at 2ϑ of 9.8° and in the range of 19.5° to 21.2° which correspond to α and β-keratin, respectively [37]. The peaks are wide because of the amorphous structure of keratin. The presence of these two peaks in the XRD pattern of EKP and

KNP confirms that no chemical change occurred after keratin extraction and nanoparticle synthesis. However, the intensity of both peaks decrease as the sample change from SCF to EKP and KNP which is due to the reduction of the particle size [38].

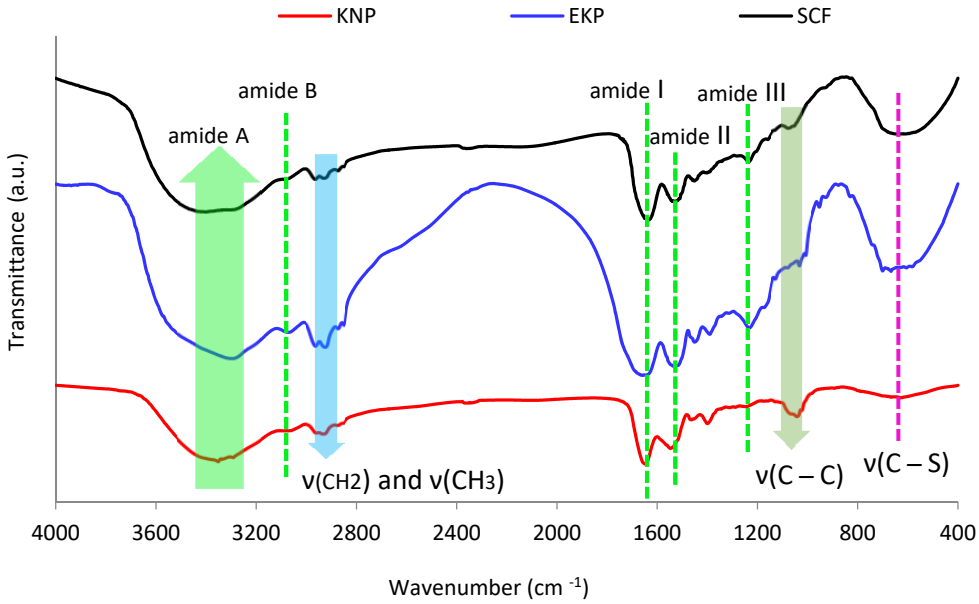

Fig. 1. FTIR spectra of SCF, extracted EKP and KNP. The presence of amide A and B as well as amide I, II and III indicate no chemical change after keratin extraction and KNP synthesis.

3.1.3. Particle size analysis

The mean hydrodynamic diameter of the KNPs was measured with a Zetasizer at different concentrations of 0.25, 0.50, 1.0, 1.5 and 3.0 g/L. The measured data are presented in Table 1. It can be seen that the KNP diameters vary in the range of 21.6 to 46.1 nm. The relationship between the particle size and concentration is complicated and not monotonic. Different parameters such as viscosity and ζ potential had an effect on this relationship. The size of the synthesized KNPs in the current research was compared with available KNP synthesis techniques in Table 2. To the best of our knowledge, the obtained nanoparticle sizes in this study are the smallest yet to be synthesized.

Table 1. The mean size and ζ potential of KNPs at different doses

Concentration (mg/ml)	Mean size (nm)	ζ potential (mV)
0.25	1.0	-33.2
0.5	29.0	-40.8
1.0	46.1	-42.9
1.5	26.6	-44.7
3.0	30.9	-59.5

Table 2. KNP size reported in different studies

Method	Reported Size
Electrospraying [39]	53 nm
Enzymatic hydrolysis [40]	215 nm
Desolvation [41]	150 nm
Phase separation and ultrasonication [42]	70 nm
The present method in this study	42 nm

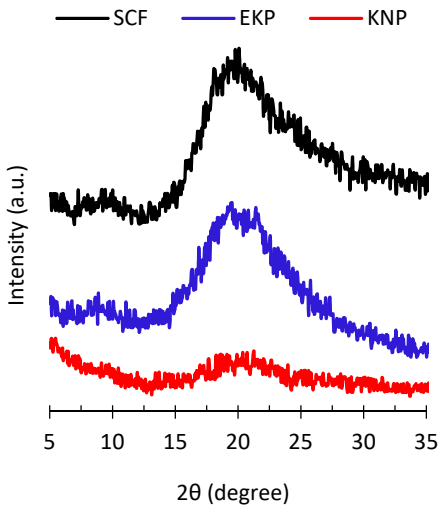

Fig. 2. XRD patterns of SCF, extracted EKP and KNP; the decrease of the intensity might be attributed to the reduction of the particle size.

3.1.4. Nanoparticle morphology

The morphology of the KNPs is shown in the TEM image in Figure 3(a). As it can be seen, the particles have an almost spherical structure. The distribution curve of the particles (Figure 3(b)) shows the mean size of the particles which is about 42±3.6 nm. This value is in good agreement with the obtained results from DLS.

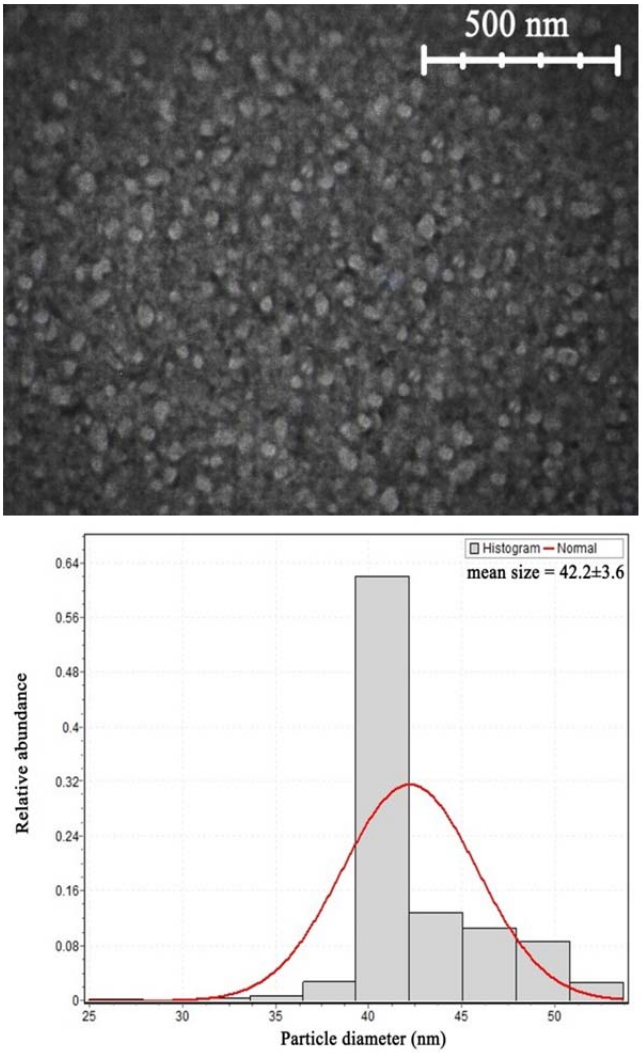

Fig.3. (a) TEM image of isolated KNPs after negative staining; the image confirms the presence of spherical nanoparticles. (b) particle size distribution of KNPs; as it can be seen KNPs have a mean diameter of 42.2±3.6 nm.

3.2. Cu (II) adsorption studies

3.2.1. Effect of adsorbent dose

Different KNP doses (0.1-5.0 g/L) were examined to investigate the relationship between adsorbent dosage and Cu (II) removal. The Cu (II) concentration in all the tests was 100 mg/L, pH was adjusted to 5, and temperature was 25°C. As it is obvious in the graph of q versus the KNP dosage in Figure 4, lower KNP doses resulted in higher adsorption capacity. However, these doses of KNP were not enough to remove any considerable amount of Cu (II). For KNP doses in the range of 0.5 to 3.0 g/L, the Cu (II) adsorption capacity was almost constant and about 30 mg/g. Considering the diagram of R (%) versus the KNP dosage in Figure 4, it seems more suitable to choose a biosorbent dosage of about 3.0 g/L due to higher Cu (II) removal since both q and R% decreased with increasing KNP concentration in the range of 3.0 to 5.0 g/L. As KNP dosage increased, more available sites and surface area were prepared; hence, Cu (II) removal increased [6,43]. However, there was a maximum value for Cu (II) removal, and the KPN inter and intra-particle interactions and its agglomeration at the concentrations higher than 3.0 g/L had reverse effects on Cu (II) removal [44,45].

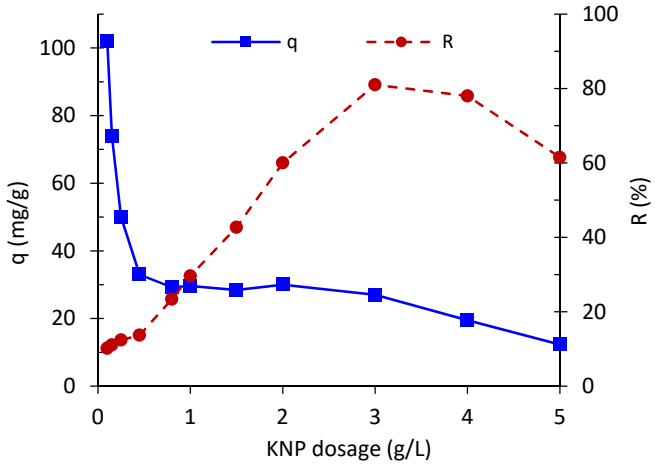

Fig.4. The effect of biosorbent dosage on adsorption capacity and removal of Cu (II) at copper concentration of 100 mg/L, pH=5, and T=25 °C.

3.2.2. Effect of initial Cu (II) concentration

The effect of the initial Cu (II) concentration (40-400 mg/L) was studied on KNP adsorption capability at three different doses: 0.15, 1.5 and 3.0 g/L. As it can be seen in Figure 5(a), the graph has two distinct regions. In the first region, Cu (II) removal increased with increasing of the initial metal concentration. This was mainly due to the higher available copper ions for adsorption [46]. Furthermore, the higher initial metal concentration caused a higher driving force which helped overcoming mass transfer resistance [47]. In the second region, Cu (II) removal decreased, which might be attributed to the adsorption site saturation [27,48]. It appeared that at a KNP dosage of 0.15 g/L, the adsorption sites were saturated even at the minimum copper concentration of 40 mg/L. Hence, the removal was almost constant. However, the adsorption capacity at a KNP dose of 0.15 g/L was much more than KNP doses of 1.5 and 3.0 g/L (Figure 5(b)), showing multilayer adsorption at the saturated sites.

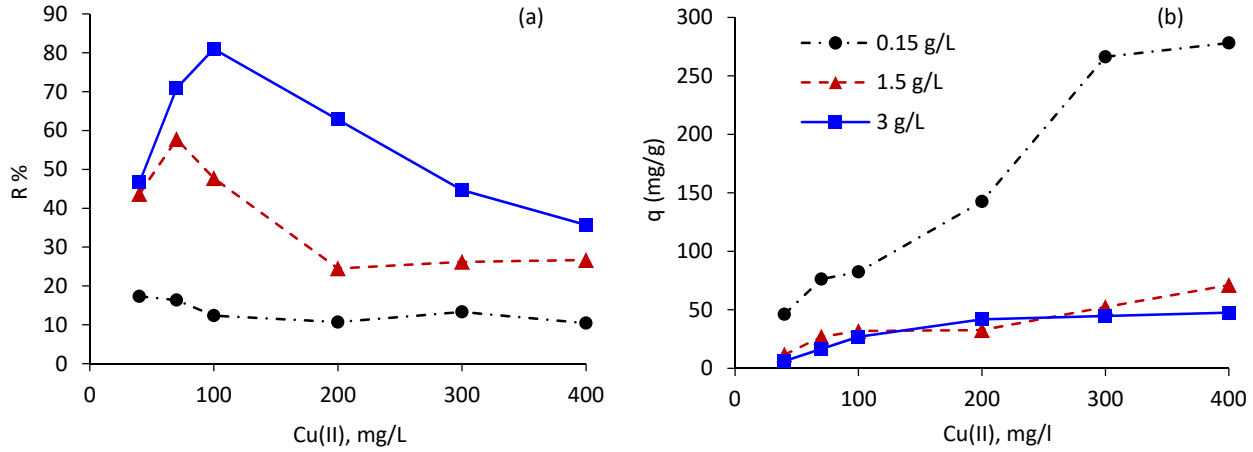

Fig. 5. The effect of initial Cu (II) concentration on (a) adsorption capacity and (b) removal of Cu(II), at three different KNP doses of 0.15, 1.5 and 3.0 g/L.

3.2.3. Adsorption isotherm

Figure 6 shows the nonlinear form of the best fitted adsorption isotherms at different KNP doses of 0.15, 1.5 and 3.0 g/L. The calculated parameters of these models are summarized in Table 4. Based on the calculated correlation coefficients, the Redlich-Peterson isotherm is best fitted to the experimental data of Cu (II) adsorption at KNP doses of 0.15 and 1.5 g/L. The exponent β_{RP} (listed in Table 4) is in the accepted range of 0-1 [49]. As the KNP dosage increases, the tendency to form a plateau increases, which confirms reaching equilibrium (Figure 6) [50].

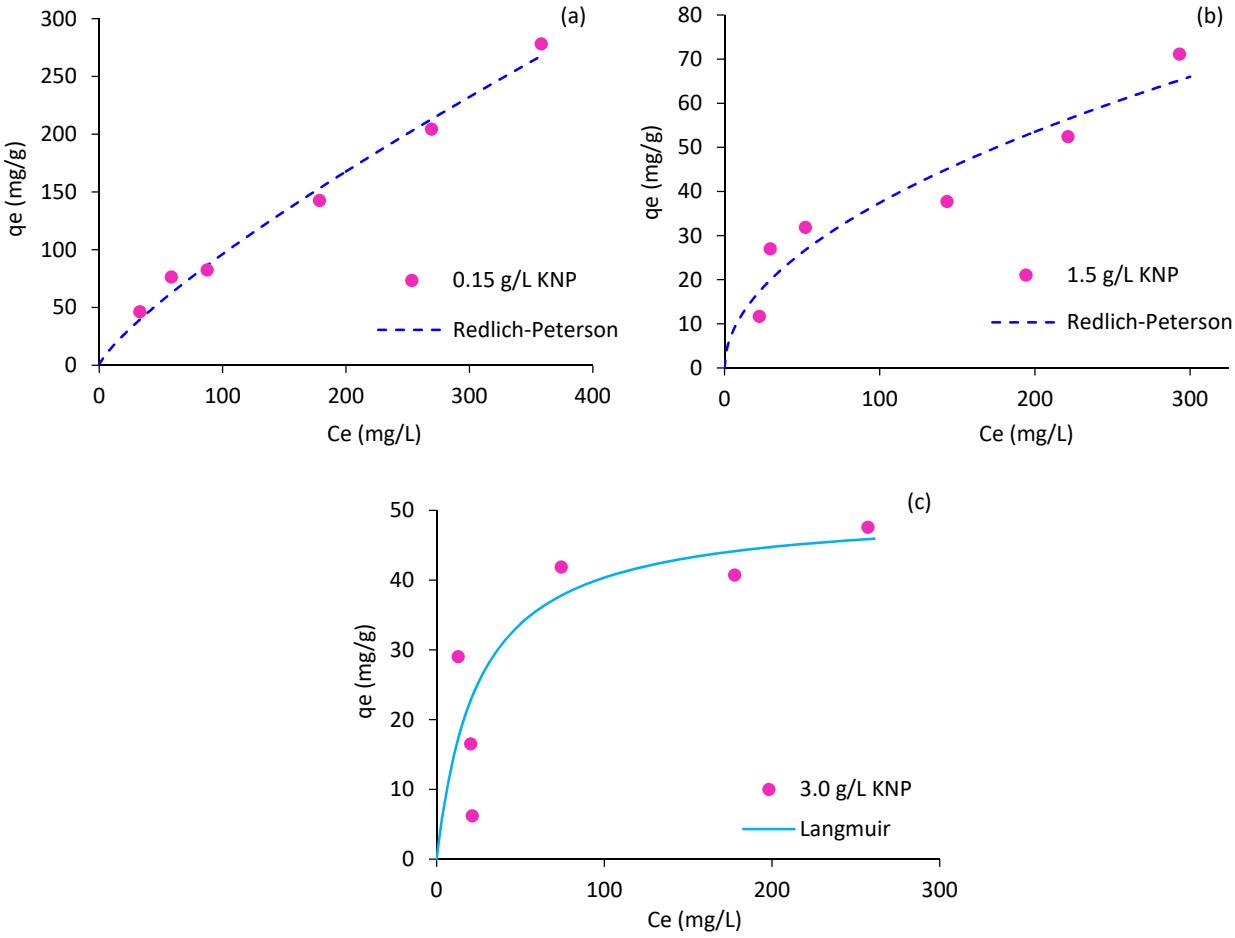

Fig. 6. The best fitted isotherm models to the experimental data.

The Langmuir model is applicable to describe the Cu (II) adsorption process at a KNP dosage of 3.0 g/L. As presented in Table 4, the Sips model could not be generated when using a KNP dose of 0.15 g/L. At a KNP dose of 1.5g/L, the data could not be explained by the Sips isotherm because of the negative value of the parameter[49]. It seems that at low KNP doses, each adsorption site can adsorb more than one Cu (II). So, the Redlich-Peterson isotherm fits the equilibrium adsorption data which is proper for heterogeneous systems. However, at higher KNP doses, more adsorption sites are provided. Hence, the adsorption isotherm changes from the Redlich-Peterson to the Langmuir model, which shows the monolayer adsorption with equal binding energy on the KNP surface. The value of the separation factor in the range of 0.06 to 0.38 indicates the favorable adsorption process ($0 < R_L < 1$). Comparing the results with other research which used keratin as a biosorbent demonstrates that the maximum adsorption capacity of KNP considerably improved in comparison to the adsorption capacity of the treated chicken feather which was about 9 mg/g [51]. The results are also in good agreement with keratin/PA6 blend nanofiber adsorption capacity (61.7-103 mg/g) [18]. The maximum Langmuir adsorption capacity KNPs for copper removal is also compared with some nanoadsorbents in Table 4.Redlich-Peterson isotherm fits the equilibrium adsorption data which is proper for heterogeneous systems. However, at higher KNP doses, more adsorption sites are provided. Hence, the adsorption isotherm changes from the Redlich-Peterson to the Langmuir model, which shows the monolayer adsorption with equal binding energy on the KNP surface. The value of the separation factor in the range of 0.06 to 0.38 indicates the favorable adsorption process ($0 < R_L < 1$). Comparing the results with other research which used keratin as a biosorbent demonstrates that the maximum adsorption capacity of KNP considerably improved in comparison to the adsorption capacity of the treated chicken feather which was about 9 mg/g [51]. The results are also in good agreement with keratin/PA6 blend nanofiber adsorption capacity (61.7-103 mg/g) [18]. The maximum Langmuir adsorption capacity KNPs for copper removal is also compared with some nanoadsorbents in Table 4.

Table 3. The calculated parameters of Langmuir, Freundlich, Sips and Redlich-Peterson isotherms at three KNP doses of (a) 0.15 g/L, (b) 1.5 g/L and (c) 3.0 g/L

Adsorption model	Parameters	KNP dose of 0.15 g/L	KNP dose of 1.5 g/L	KNP dose of 3.0 g/L
Langmuir		556	85	50
		2.3	10.8	40.8
		0.52-0.91	0.19-0.70	0.06-0.38
		0.75	0.88	0.98
Freundlich	n	1.4	1.9	4
		3.7	3.3	11.5
		0.98	0.84	0.62
Sips		-	0.24	0.20
		-	3.52×10^{-3}	1.61
		-	-0.98	4.06×10^{-3}
		-	-	68
		-	-	0.81
Redlich-Peterson	K_{RP}	3.19×10^{6}	4.22×10^{6}	1.66
		0.20	0.48	0.95
		1.33×10^{6}	1.22×10^{6}	0.04
		0.99	0.95	0.80

3.2.4. Adsorption kinetics

The pseudo-first order, pseudo-second order and intra-particle diffusion models were applied to investigate the adsorption kinetics of Cu (II) with KNPs. The fitted models are shown in Figure 7. As the value of the correlation coefficient (R^2) and the difference between the calculated adsorption capacity ($q_{e,cal}$) and the experimental one ($q_{e,exp}$) suggested, the pseudo-first order kinetic model (Figure 7(a)) did not fit the experimental data. However, this model is usually useful to describe the adsorption kinetics at the initial time steps. As it is shown in Figure 7c, the plotted intra-particle diffusion model (Figure 7(b)) had two distinct steps. The first linear region represented intra-particle diffusion, and the second one represented the adsorption-desorption equilibrium [57]. It seems that the nano-size, the large surface area and the negative surface charge of KNPs caused the fast adsorption of copper ions. Hence, the intra particle diffusion was not a rate limiting step in this process. Based on the correlation coefficient listed in Table 5, the pseudo-second order kinetic model (Figure 7(c)) was best fitted to the experimental data. The

calculated adsorption capacity ($q_{e,cal}$) of this model was also in good agreement with the experimental one ($q_{e,exp}$). This model assumed chemical sorption as a rate-limiting step in the process of metal ion adsorption and involved electron exchange between Cu (II) and KNP as a biosorbent [31].

Table 4. The reported maximum Langmuir adsorption capacity of different nanoadsorbents for copper removal

nanoadsorbent	q_m (mg/g)	pH	Temperature (K)	Adsorbent dosage (g/L)	Ref.
anatase nanoadsorbent	23.74	6	298	0.15	[52]
chitosan-bound Fe_3O_4 magnetic nanoparticles	21.5	5	300	21	[53]
gum Arabic modified magnetic nano-adsorbent	35.5	5	298	5	[54]
amino-functionalized magnetic nano-adsorbent	12.43	5	298	20	[55]
Fe_3O_4 magnetic nanoparticles coated with humic acid	46.3	6	298	1	[56]
chitosan-coated magnetic nanoparticles modified with α-ketoglutaric acid	91.15	6	298	5	[4]
amino-functionalized magnetic nanoparticles	25.77	6	298	0.1	[3]
Carboxymethyl-β-cyclodextrin conjugated magnetic nanoparticles	47.2	6	298	12	[8]
KNPs	50	5	298	3	Current research

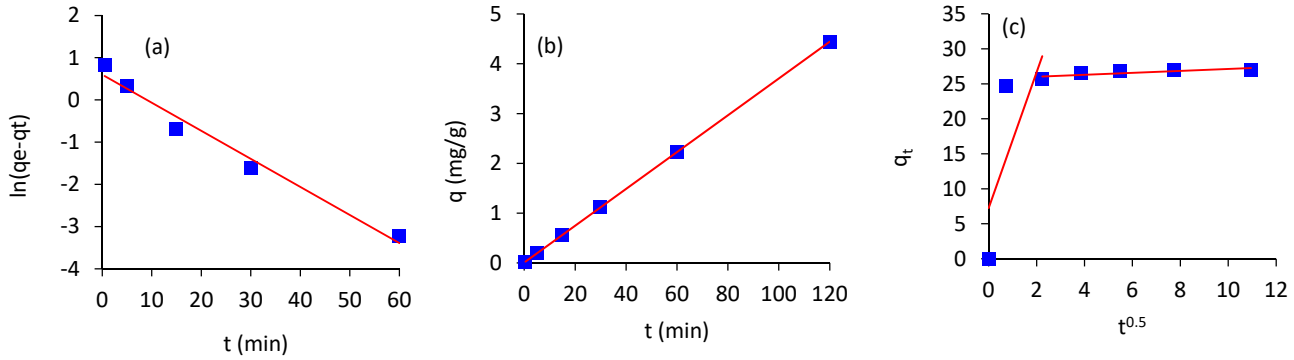

Fig. 7. The linear forms of (a) pseudo-first, (b) pseudo-second and (c) intra-particle diffusion models fitted with experimental data. The pseudo-second order kinetic model fits the experimental data best, showing chemisorption as a rate-limiting step in the adsorption process.

3.2.5. Desorption of Cu (II)

The precipitated KNPs after Cu (II) adsorption were separated via centrifugation (3.0 g/L KNP; 100 mg/L Cu (II)). They were then treated with 1% acetic acid for an hour. The number of hydrogen ions increased as the pH value decreased, resulting in the hydrogen ions replacement with Cu (II) ions and KNP-NH_3^+ formation. The amount of released Cu (II) was measured using AAS. The desorption ratio was calculated by dividing the value of the desorbed Cu (II) into the acetic acid solution to the value of the adsorbed metal onto the KNPs. The ratio of 86% was achieved at this desorption condition.

Table 5. The calculated parameters of pseudo-first, pseudo-second and intra-particle diffusion models

Kinetic model	Parameters	Value
		27.0
Pseudo-first order	$q_{e.cal}$	4.0
		8.5×10^{-3}
		0. 8
Pseudo-second order	$q_{e.cal}$	27.0
		0.2
		1.0
Intra-particle diffusion — The first region		9.7
		7.2
		0.8
Intra-particle diffusion — The second region		6.5×10^{-2}
		26.3
		0.9

3.2.6. SCF and KNP adsorption efficiency of Cu (II)

Various experiments were performed for the comparison of SCF and KNP efficiency for Cu (II) removal. The biosorbent dose in all experiments was 3.0 g/L, Cu (II) concentration was 100 mg/L, pH was 5 and the temperature was 25 °C. The SCF adsorption capacity was

about 8.5 mg/g, while the KNP capacity for Cu (II) removal was about 30 mg/g. The higher value of KNP adsorption capacity might be attributed to the size reduction of the KNPs, leading to more functional groups becoming available on the KNP surface and adsorbing Cu (II). However, SCF functional groups were involved in inter and intra-molecular interactions and they were not free to adsorb metal ions.

4. Conclusions

In the present research, a straightforward method was used to synthesize the keratin nanoparticles of about 42 nm. The produced nanoparticles were characterized with FTIR, XRD and DLS analysis. The results indicated the presence of the original functional groups in the synthesized nanoparticles and no significant structural change. The DLS analysis also confirmed the negative surface charge of KNPs, which was low enough (< -30 mV) to stabilize KNP dispersion. The KNPs were then applied for Cu (II) removal from aqueous solutions. The experiments revealed that the KNP dosage of 3.0 g/L resulted in better Cu (II) uptake. At this dosage, the Langmuir isotherm with a maximum adsorption capacity of 50 mg/g fitted best, indicating monolayer adsorption. However, at lower KNP doses of 0.15 and 1.5 g/L, the Redlich-Peterson adsorption isotherm fitted the data, showing multilayer adsorption. The pseudo-second order kinetic model was best fitted to the experimental data which indicated that chemisorption was the dominant phenomena during the adsorption process. Considering these results, the synthesized KNPs seems to be applicable for Cu (II) removal from contaminated water.

References

[1] Farooq, U., Kozinski, J. A., Khan, M. A., Athar, M. (2010). Biosorption of heavy metal ions using wheat based biosorbents–A review of the recent literature. *Bioresource technology*, *101*(14), 5043-5053.

[2] Asthana, A., Verma, R., Singh, A. K., Susan, M. A. B. H. (2016). Glycine functionalized magnetic nanoparticle entrapped calcium alginate beads: a promising adsorbent for removal of Cu (II) ions. *Journal of environmental chemical engineering*, *4*(2), 1985-1995.

[3] Hao, Y. M., Man, C., Hu, Z. B. (2010). Effective removal of Cu (II) ions from aqueous solution by amino-functionalized magnetic nanoparticles. *Journal of hazardous materials*, *184*(1-3), 392-399.

[4] Zhou, Y. T., Nie, H. L., Branford-White, C., He, Z. Y., Zhu, L. M. (2009). Removal of Cu2+ from aqueous solution by chitosan-coated magnetic nanoparticles modified with α-ketoglutaric acid. *Journal of colloid and interface science*, *330*(1), 29-37.

[5] Almohammadi, S., Mirzaei, M. (2016). Removal of copper (II) from aqueous solutions by adsorption onto granular activated carbon in the presence of competitor ions. *Advances in Environmental Technology*, 2(2), 85-94.

[6] Vijayalakshmi, K., Gomathi, T., Latha, S., Hajeeth, T., Sudha, P. N. (2016). Removal of copper (II) from aqueous solution using nanochitosan/sodium alginate/microcrystalline cellulose beads. *International journal of biological macromolecules*, *82*, 440-452.

[7] Edition, F. (2011). Guidelines for drinking-water quality. *WHO chronicle*, *38*(4), 104-8

[8] Badruddoza, A. Z. M., Tay, A. S. H., Tan, P. Y., Hidajat, K., Uddin, M. S. (2011). Carboxymethyl-β-cyclodextrin conjugated magnetic nanoparticles as nano-adsorbents for removal of copper ions: synthesis and adsorption studies. *Journal of hazardous materials*, *185*(2-3), 1177-1186.

[9] Song, J., Kong, H., Jang, J. (2011). Adsorption of heavy metal ions from aqueous solution by polyrhodanine-encapsulated magnetic nanoparticles. *Journal of colloid and interface science*, *359*(2), 505-511.

[10] Khan, T. A., Singh, V. V. (2010). Removal of cadmium (II), lead (II), and chromium (VI) ions from aqueous solution using clay. *Toxicological and environ chemistry*, *92*(8), 1435-1446.

[11] Ngah, W. W., Endud, C. S., Mayanar, R. (2002). Removal of copper (II) ions from aqueous solution onto chitosan and cross-linked chitosan beads. *Reactive and functional polymers*, *50*(2), 181-190

[12] Khan, T. A., Mukhlif, A. A., Khan, E. A., Sharma, D. K. (2016). Isotherm and kinetics modeling of Pb (II) and Cd (II) adsorptive uptake from aqueous solution by chemically modified green algal biomass. *Modeling earth systems and environment*, *2*(3), 117.

[13] Khan, T. A., Nazir, M., Khan, E. A. (2016). Magnetically modified multiwalled carbon nanotubes for the adsorption of bismarck brown R and Cd (II) from aqueous solution: batch and column studies. *Desalination and water treatment*, *57*(41), 19374-19390.

[14] Tonin, C., Aluigi, A., Varesano, A., Vineis, C. (2010). Keratin-based nanofibres. In *Nanofibers*. InTech.

[15] Aguayo-Villarreal, I. A., Bonilla-Petriciolet, A., Hernández-Montoya, V., Montes-Morán, M. A., Reynel-Avila, H. E. (2011). Batch and column studies of Zn2+ removal from aqueous solution using chicken feathers as sorbents. *Chemical engineering journal*, *167*(1), 67-76.

[16] Mittal, A. (2006). Adsorption kinetics of removal of a toxic dye, Malachite Green, from wastewater by using hen feathers. *Journal of hazardous materials*, *133*(1-3), 196-202.

[17] Khosa, M. A., Wu, J., Ullah, A. (2013). Chemical modification, characterization, and application of chicken feathers as novel biosorbents. *Rsc Advances*, *3*(43), 20800-20810.

[18] Aluigi, A., Tonetti, C., Vineis, C., Tonin, C., Mazzuchetti, G. (2011). Adsorption of copper (II) ions by keratin/PA6 blend nanofibres. *European polymer journal*, *47*(9), 1756-1764.

[19] Khosa, M. A., Ullah, A. (2014). In-situ modification, regeneration, and application of keratin biopolymer for arsenic removal. *Journal of hazardous materials*, *278*, 360-371.

[20] Dutta, J. (2005). Nanotechnology in environmental protection and pollution. *Science and technology of advanced materials*, *6*(3-4), 219.

[21] Nomura, Y., Aihara, M., Nakajima, D., Kenjou, S., Tsukuda, M., Tsuda, Y. (2007). *U.S. Patent Application No. 10/594,758*.

[22] Bertagnolli, C., Grishin, A., Vincent, T., Guibal, E. (2016). Recovering heavy metal ions from complex solutions using polyethylenimine derivatives encapsulated in alginate matrix. *Industrial engineering chemistry research*, *55*(8), 2461-2470.

[23] Sheng, P. X., Ting, Y. P., Chen, J. P., Hong, L. (2004). Sorption of lead, copper, cadmium, zinc, and nickel by marine algal biomass: characterization of biosorptive capacity and investigation of mechanisms. *Journal of colloid and interface science*, *275*(1), 131-141.

[24] Gao, B., An, F., Liu, K. (2006). Studies on chelating adsorption properties of novel composite material polyethyleneimine/silica gel for heavy-metal ions. *Applied surface science*, *253*(4), 1946-1952.

[25] Khosa, M. A., Ullah, A. (2014). In-situ modification, regeneration, and application of keratin biopolymer for arsenic removal. *Journal of hazardous materials*, *278*, 360-371.

[26] Langmuir, I. (1916). The constitution and fundamental properties of solids and liquids. Part I. Solids.*Journal of the American chemical society*, *38*(11), 2221-2295.

[27] Freundlich, U. (1906). Uber die adsorption in lusungen. Zeitschrift für physikalische chemie, 57, 385-470.

[28] Redlich, O. J. D. L., Peterson, D. L. (1959). A useful adsorption isotherm. *Journal of physical chemistry*, *63*(6), 1024-1024.

[29] Sips, R. (1948). On the structure of a catalyst surface. *The journal of chemical physics*, *16*(5), 490-495.

[30] Lagergren, S. (1898). Zur theorie der sogenannten adsorption geloster stoffe. *Kungliga svenska vetenskapsakademiens. Handlingar*, *24*, 1-39.

[31] Ho, Y. S., McKay, G. (1999). Pseudo-second order model for sorption processes. *Process biochemistry*, *34*(5), 451-465.

[32] Weber, W. J., Morris, J. C. (1963). Kinetics of adsorption on carbon from solution. *Journal of the sanitary engineering division*, *89*(2), 31-60.

[33] Stuart, B. (2005). Infrared spectroscopy. *Kirk-Othmer Encyclopedia of Chemical Technology*. ACS Pub.

[34] Sun, P., Liu, Z. T., Liu, Z. W. (2009). Particles from bird feather: A novel application of an ionic liquid and waste resource. *Journal of hazardous materials*, *170*(2-3), 786-790.

[35] Ha, S. W., Tonelli, A. E., Hudson, S. M. (2005). Structural studies of bombyx m ori silk fibroin during regeneration from solutions and wet fiber spinning. *Biomacromolecules*, *6*(3), 1722-1731.

[36] Shao, J., Zheng, J., Liu, J., Carr, C. M. (2005). Fourier transform Raman and Fourier transform infrared spectroscopy studies of silk fibroin. *Journal of applied polymer science*, *96*(6), 1999-2004.

[37] Xie, H., Li, S., Zhang, S. (2005). Ionic liquids as novel solvents for the dissolution and blending of wool keratin fibers. *Green chemistry*, *7*(8), 606-608.

[38] Cullity, B. D. (1978). *Elements of X-ray diffraction*, 2nd Ed., Addison-Wesley Pub. Co, USA.

[39] Rad, Z. P., Tavanai, H., Moradi, A. R. (2012). Production of feather keratin nanopowder through electrospraying. *Journal of aerosol science*, *51*, 49-56.

[40] Eslahi, N., Dadashian, F., Nejad, N. H. (2013). Optimization of enzymatic hydrolysis of wool fibers for nanoparticles production using response surface methodology. *Advanced powder technology*, *24*(1), 416-426.

[41] Saravanan, S., Sameera, D. K., Moorthi, A., Selvamurugan, N. (2013). Chitosan scaffolds containing chicken feather keratin nanoparticles for bone tissue engineering. *International journal of biological macromolecules*, *62*, 481-486.

[42] Xu, H., Shi, Z., Reddy, N., Yang, Y. (2014). Intrinsically water-stable keratin nanoparticles and their in vivo biodistribution for targeted delivery. *Journal of agricultural and food chemistry*, *2*(37), 9145-9150.

[43] Mall, I. D., Srivastava, V. C., Agarwal, N. K. (2006). Removal of Orange-G and Methyl Violet dyes by adsorption onto bagasse fly ash—kinetic study and equilibrium isotherm analyses. *Dyes and pigments*, *69*(3), 210-223.

[44] Brown, P. A., Gill, S. A., Allen, S. J. (2000). Metal removal from wastewater using peat. *Water research*, *34*(16), 3907-3916.

[45] Shukla, A., Zhang, Y. H., Dubey, P., Margrave, J. L., Shukla, S. S. (2002). The role of sawdust in the removal of unwanted materials from water. *Journal of hazardous materials*, *95*(1-2), 137-152.

[46] Ki, C. S., Gang, E. H., Um, I. C., Park, Y. H. (2007). Nanofibrous membrane of wool keratose/silk fibroin blend for heavy metal ion adsorption. *Journal of membrane science*, *302*(1-2), 20-26.

[47] Das, D., Basak, G., Lakshmi, V., Das, N. (2012). Kinetics and equilibrium studies on removal of zinc (II) by untreated and anionic surfactant treated dead biomass of yeast: Batch and column mode. *Biochemical engineering journal*, *64*, 30-47.

[48] Langmuir, I. (1918). The adsorption of gases on plane surfaces of glass, mica and platinum. *Journal of the American chemical society*, *40*(9), 1361-1403.

[49] Tran, H. N., You, S. J., Hosseini-Bandegharaei, A., Chao, H. P. (2017). Mistakes and inconsistencies regarding adsorption of contaminants from aqueous solutions: a critical review. *Water research*, *120*, 88-116.

[50] Belhachemi, M., Addoun, F. (2011). Comparative adsorption isotherms and modeling of methylene blue onto activated carbons. *Applied water science*, *1*(3-4), 111-117.

[51] Al-Asheh, S., Banat, F. (2003). Beneficial reuse of chicken feathers in removal of heavy metals from wastewater. *Journal of cleaner production*, *11*(3), 321-326.

[52] Kocabaş-Ataklı, Z. Ö., Yürüm, Y. (2013). Synthesis and characterization of anatase nanoadsorbent and application in removal of lead, copper and arsenic from water. *Chemical engineering journal*, *225*, 625-635.

[53] Chang, Y. C., Chen, D. H. (2005). Preparation and adsorption properties of monodisperse chitosan-bound Fe_3O_4 magnetic nanoparticles for removal of Cu (II) ions. *Journal of colloid and interface science*, *283*(2), 446-451.

[54] Banerjee, S. S., Chen, D. H. (2007). Fast removal of copper ions by gum Arabic modified magnetic nano-adsorbent. *Journal of hazardous materials*, *147*(3), 792-799.

[55] Huang, S. H., Chen, D. H. (2009). Rapid removal of heavy metal cations and anions from aqueous solutions by an amino-functionalized magnetic nano-adsorbent. *Journal of hazardous materials*, *163*(1), 174-179.

[56] Liu, J. F., Zhao, Z. S., Jiang, G. B. (2008). Coating Fe_3O_4 magnetic nanoparticles with humic acid for high efficient removal of heavy metals in water. *Environmental science and technology*, *42*(18), 6949-6954.

[57] Guo, S., Jiao, P., Dan, Z., Duan, N., Chen, G., Zhang, J. (2017). Preparation of L-arginine modified magnetic adsorbent by one-step method for removal of Zn (Ⅱ) and Cd (Ⅱ) from aqueous solution. *Chemical engineering journal*, *317*, 999-1011.